Article:
Vaitkunaite, G, Espejo, C, Wang, C et al. (2020) MoS_2 tribofilm distribution from low viscosity lubricants and its effect on friction. Tribology International, 151. 106531. ISSN: 0301-679X

https://doi.org/10.1016/j.triboint.2020.106531

MoS_2 TRIBOFILM DISTRIBUTION FROM LOW VISCOSITY LUBRICANTS AND ITS EFFECT ON FRICTION

G. Vaitkunaite [a*], C. Espejo [a], C. Wang [a], B. Thiebaut [b], C. Charrin [b], A. Neville [a], A. Morina [a]
*mngv@leeds.ac.uk,
[a] School of Mechanical Engineering, University of Leeds, Leeds LS2 9JT, UK,
[b] TOTAL, Solaize Researcher Center, BP22-69360 Cedex, France.

ABSTRACT

The current study analyses the friction performance of low viscosity fully-formulated oils containing the Molybdenum Dialkyl Dithiocarbamate (MoDTC) friction modifier at different concentrations. The MoDTC friction modifier is known to produce MoS_2 sheets in the tribocontact providing a low coefficient of friction under boundary lubrication conditions. However, there is a little knowledge around the quantitative relationship between the concentration of MoDTC in the oil and MoS_2 amount and distribution in the contact. The study uses Raman spectroscopy mapping capability to characterise the tribofilm formed from different chemistry lubricants and under different tribological conditions as defined by the lambda ratio. After qualitative and quantitative chemical surface characterisation a discussion is presented to highlight some important aspects to relate the formed MoS_2 sheets, their spatial distribution in tribofilms and the subsequent tribological performance.

1. INTRODUCTION

According to the European Environment Agency and U.S. Environmental Protection Agency, 30% of greenhouse gas emissions are due to transportation activities [1, 2]. Energy savings in internal combustion engines are of most importance and can be reached by improving lubricant performance by lowering lubricant viscosity and adding friction and anti-wear additives in addition to adjusting surface roughness of rubbing components [3]. Therefore market demands are pushing internal combustion engines to more severe operating conditions. Thinning of the lubricant film and overheating are experienced in engine components due to extreme operating conditions. Therefore, future engine oils have to deliver high performance in both engine starting and stopping stages to protect component surfaces from wear as well as to reduce the friction in the rubbing contacts.

Engine oils have moved towards lower viscosity products to reduce energy losses in fluid film lubrication, leading to lower energy losses in tribological engine components such as oil pumps, bearings, and pistons [4, 5]. However, reduction of oil viscosity also increases the severity of the contact in the boundary lubrication regime. As a result, more severe contacts are seen in engine components, especially in the cylinder block assembly leading to higher friction and wear in the top dead and bottom dead centre areas at the reversal points of the piston ring stroke [6]. Oil viscosity reduction leads to a decrease in oil load-carrying capacity and, as a result, greater friction losses are experienced in the piston ring and liner contacts in the engine [6]. Friction and wear in boundary lubrication are primarily determined by the chemical properties of the lubricant, where important features are solvency, dispersion, detergency, anti-wear, anti-corrosion, frictional properties and antioxidant capacity [7, 8]. Some of these properties are provided by the base oil mixture, and others are introduced separately as additives in the oil blend [9].

MoDTC is found to be beneficial for engine lubrication; in the boundary lubrication regime MoDTC chemical bonds rupture and form 2D lateral MoS_2 nano-sheets. Due to MoS_2 sheet formation in the tribological contact area, the reduction of the coefficient of friction values occurs [10-14]. MoDTC decomposition and MoS_2 tribofilm formation can be influenced by many factors like oil formulation chemistry [14, 15], tribological contact conditions such as surface roughness [16], texturing [17, 18], temperature [12] and interacting surface materials [19-21].

Raman spectroscopy is found to be one of the most suitable techniques to determine the presence of MoS_2 vibrational modes which appear as distinct peaks at 383 cm^{-1} and 408 cm^{-1} Raman shift, equivalent to A_{1g} and E^1_{2g} vibrational modes [11-13]. Xu et. al. [10] combined Atomic Force Microscopy (AFM) and Raman

spectroscopy to quantify the MoS_2 tribofilm distribution and thickness, correlating the friction behaviour with MoS_2 tribofilm formation and removal. In their work, they used the coverage of MoS_2 as a measure of the tribofilm ability to reduce friction. In Fig. 1 their results are presented and it is clear that when MoS_2 coverage increases there is a corresponding decrease in the friction coefficient. There is some evidence in the work of Xu et al. [10] that the friction and coverage reach a plateau at between 0.055-0.058 and 75-80% respectively and at this point the total intensity from the Raman peak continues to increase. The work demonstrated that Raman spectroscopy has a unique place in the study of tribofilms and raised the question about what parameter relating to MoS_2 impacts the friction and tribological performance: the surface coverage or the total amount of MoS_2 in the tribocontact. This is not a trivial question to answer and this paper presents a further analysis that makes a contribution in this area.

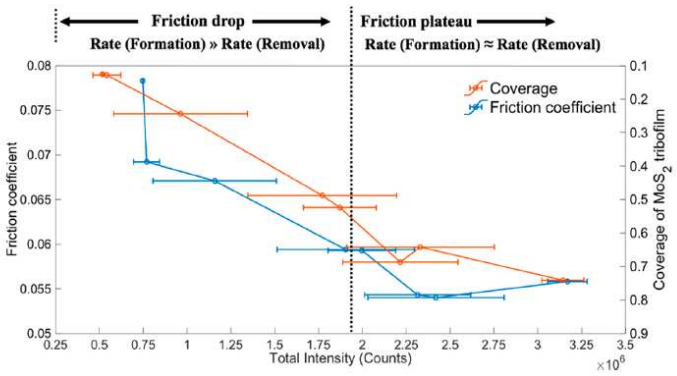

Fig. 1. a) Schematic diagram of the MoDTC derived tribofilm evolution [10].

It is still not well known how fully-formulated oil chemistry influences MoDTC decomposition and MoS_2 nano-sheet formation and their spatial distribution. MoDTC interaction with fully-formulated oil components, such as anti-wear additives, viscosity index improvers, detergents and dispersants and synergetic and antagonistic effects towards friction reduction behaviour and tribofilm growth influence have not been widely reported [22, 23]. With a growing demand for friction reduction in engine components through low viscosity engine lubricants, polymeric viscosity index improvers are also very important.

One of the most common ways to adjust base oil fluid viscosity is to add polymeric viscosity modifiers (VM) to the engine oil to lower lubricating film thinning at high temperatures and assure liquid flow. A typical star-shaped poly-isoprene styrene hydrogenated polymeric viscosity modifier chemical formula and molecular structure is shown in Fig. 2.

a) **b)**

Fig. 2. a) Chemical formula of poly-isoprene styrene hydrogenated polymer, b) the molecular structure of polymer arms connected to a central core [24-26].

Star-shaped poly-isoprene styrene hydrogenated polymer physico-chemistry properties and friction behaviour have previously been researched in elastohydrodynamic lubrication conditions when fluid film-forming thickness is most important [24, 25]. A strong correlation between oil rheology properties and physico-chemistry of base oil and viscosity modifiers, especially with regard to film-forming capacity was shown [24, 25]. It proves that tribological behaviour is linked to the oil properties at a molecular level and polymer conformation. However, there is a lack of knowledge on the influence that polymeric viscosity modifiers have on friction behaviour and tribofilm formation in the boundary regime in fully-formulated low viscosity oils.

The current paper aims to study the effect of MoDTC and low viscosity fully-formulated oils and to establish

a Raman spectroscopy based quantitative method for local MoS_2 amount characterisation, to fully understand the friction reduction performance and its link to the MoS_2 quality and quantity.

2. EXPERIMENTAL METHODOLOGY

2.1 Tribological tests

Experimental tests were conducted using low viscosity fully-formulated (FF) oils with different viscosity modifier content and base oil ratios, keeping the rest of the oil chemical composition constant. Oils are blended with 0.2, 0.5, 0.7 and 1 wt% MoDTC friction modifier and tested in the boundary lubrication regime using a ball-on-disk tribometer using lambda ratio values close to the ones occurring in internal combustion engines. Friction behaviour is then correlated according to the MoDTC content in a fully-formulated oil and the lambda ratio.

Raman spectroscopy was used to characterise spatial distribution of the MoS_2 formed in the tribofilm on the steel sample wear tracks. The friction performance of each of the oils is linked to the physical and chemical properties of MoS_2 tribofilm formed on the wear scar and the rheology of the fully-formulated low viscosity oil.

The experimental tests were conducted in a uni-directional ball-on-disk custom-built liquid cell. The liquid cell with an external heating block was adapted to the Bruker UMT-TriboLab tester rotary motor. The cell configuration and the resulting tribological contact scheme are shown in Fig.3. The disk-shaped sample is fixed to the lower rotary drive and load is applied on the ball sample by the upper assembly, which is fixed to a strain-gauge force sensor. The sample platform is submerged in an oil bath and sealed with a cap to avoid contamination. An external induction heating block was used to keep the oil temperature constant.

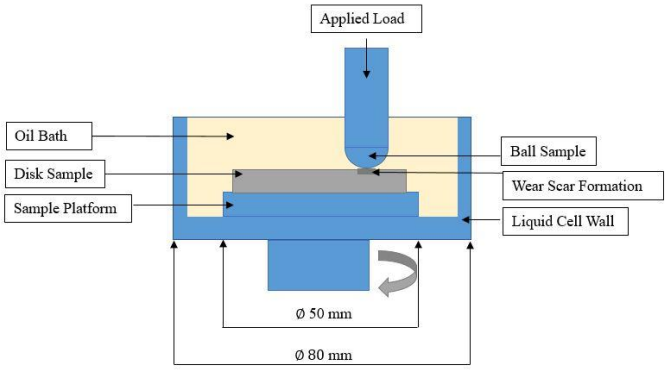

Fig. 3. Tribological contact schematic created in the uni-directional ball-on-disk custom-built liquid cell

When the load is applied on the sample surface, the strain-gauge force sensor converts physical displacement into an electrical signal. The signal is digitised and used by the TriboLab software to calculate the vertical and lateral forces exerted on the sample surface. Data feed is collected through F_x (lower rotary drive) and F_z (force sensor) channels. To acquire COF values in real-time acquisition F_x (friction force) data feed is divided by F_z (normal load). During the tests, friction, time and distance were recorded. The final COF value was obtained by averaging the recorded values of the last 20 minutes of the test. The stabilisation time is calculated as the time needed for the friction drop to occur and for a stable friction regime to be reached for the particular tribological conditions.

Data filter width is the number of acquired friction data points averaged of each data point displayed on the graph. For these tests filter width was set 100, which gives 100 data points per second. The calibration procedure mentioned above were kept constant for all ball-on-disk tests.

2.2 Materials, oils and testing conditions

The ball samples were AISI 52100 high carbon bearing steel, known for good anti-wear properties and disk washers AISI 1050 medium carbon steel. The materials properties are given in Table 1. Sample surfaces were measured with Taylor Hobson 120L Talysurf contact profilometer with 2 μm conical-shaped diamond stylus.

Roughness values (R_a) were acquired tracking a 5 mm profile across the sample. Three measurements were taken per sample and added into the calculation for initial the lambda ratio estimations. The average measured roughness values are supplied in Table 1. Before testing the samples were rinsed with heptane and cleaned in an ultrasonic bath for 10 minutes.

Table 1. Materials data of the ball and disk samples used in the unidirectional ball-on-disk testing

	Disk	Ball
Sample dimensions	Outer Diameter 42 mm Inner Diameter 25 mm Thickness 1 mm	Diameter 12.7 mm
Material	AISI 1050	AISI 52100
Poisson ratio	0.27-0.3	
Young modulus	190-210 GPa	
Hardness (HRC)	50-62	60-67
Surface roughness (R_a)	0.125 μm	0.01 μm

Chemical components for fully-formulated oils were supplied by TOTAL and blended according to the established procedure. Three oil blends were prepared to analyse the influence of oil viscosity on friction behaviour. The base oil fluids for all three blends were made by combining API group III hydrocracked mineral oil and API group IV PAO synthetic oil at different ratios. Detergents, dispersants, antioxidants, anti-wear, and anti-corrosion additives were added into the mixture as an additive package. The additive package amount was kept constant in all oil blends.

Poly-isoprene styrene hydrogenated polymer was added to modify the viscosity of the tested oils. After blending the oils, the dynamic viscosity was measured with a Malvern Kinexus Pro+ Rheometer. Dynamic viscosity measurements were taken at 90°C and 100°C temperatures in a 500 s^{-1} shear rate. The final dynamic viscosity value at each temperature is the average of 60 measurements. High Temperature High Shear (HTHS) tests were conducted according to ASTM D4683 at 150°C. The viscosity values are presented in Table 2. Fully-formulated oil 1 has no additional viscosity improver. Fully-formulated oil 2 has the same base oil viscosity as oil 1 and contains an additional viscosity modifier. Fully-formulated oil 3 has the highest base oil viscosity mixed with additional viscosity modifier.

MoDTC was added to each blend in concentrations of 0.2, 0.5, 0.7 and 1 wt%, which is equivalent of 200 ppm to 1000 ppm of molybdenum. Fully-formulated oil blends chemistries and viscosities are summarised in Table 2. MoDTC concentration influence on the fully-formulated oil blend viscosity is very small as mentioned in previously conducted studies [10].

Table 2. Oil formulation and viscosities

	FF Oil 1	FF Oil 2	FF Oil 3
Viscosity modifier (wt, %)	-	4 wt%	4.2 wt%
Kinematic viscosity of the base oil at 100°C (cSt)	3	3	5.1
HTHS at 150°C (cP)	1.7	2.1	3
Pressure-Viscosity Coefficient, GPa^{-1}	9.7	9.7	11.7
Dynamic viscosity at 90°C (η_o, Pa s)	$4.15 \cdot 10^{-3}$	$5.76 \cdot 10^{-3}$	$9.12 \cdot 10^{-3}$
Dynamic viscosity at 100°C (η_o, Pa s)	$3.42 \cdot 10^{-3}$	$4.76 \cdot 10^{-3}$	$7.33 \cdot 10^{-3}$
MoDTC concentration (wt%)	0.2% - 1%	0.2% - 1%	0.2% -1%

An overview of testing conditions is given in Table 3. The test duration was one hour, which resulted in 220 m, 340 m and 680 m sliding distances for 40 rpm, 60 rpm, 120 rpm speeds respectively. Boundary lubrication conditions were selected to be typically in the range of those occurring in the engine. Tribometer tests were conducted at 90°C and Hertzian contact pressure of 0.72 GPa. The speeds were changed from 40 rpm (0.065 m/s) to 120 rpm (0.2 m/s) resulting in the initial the lambda ratio range 0.15 to 0.3. Dowson and Higginson expression [27-29] was used to calculate minimum film thickness (h_{min}) in Equation (1) and the lambda ratio (λ) according to Equation (2) where R* is the radius of curvature (m), U - the entrainment speed (m/s), E* - the

reduced Young's modulus (Pa), η_0 - the dynamic viscosity of the oil (Pa s), α - the pressure-viscosity coefficient (Pa^{-1}), W - applied load (N), $R_{a(1)}$ and $R_{a(2)}$ are the surface roughnesses of the rubbing surfaces. Tests were repeated at least two to four times and the percentage error did not exceed 5.3% of the mean value.

$$\frac{h_{min}}{R^*} = 3.63\left(\frac{U\eta_0}{E^*R^*}\right)^{0.68}(\alpha E^*)^{0.49}\left(\frac{W}{E^*R^*}\right)^{-0.073}(1-e^{-0.68k}); (1) \qquad \lambda = \frac{h_{min}}{\sqrt{{R_{a(1)}}^2 + {R_{a(2)}}^2}}; (2)$$

Table 3. Tribometer testing parameter

Constant parameters									
Hertzian pressure	0.72 GPa								
Wear track radius (mm)	15 mm								
Oil temperature	90°C								
Test duration	1 h								
Changing parameters									
Speed (rpm)	40			60			120		
Linear speed (m/s)	0.065			0.1			0.2		
Test distance (m)	220			340			680		
Oil type	FF1	FF2	FF3	FF1	FF2	FF3	FF1	FF2	FF3
Initial the lambda ratio	0.12	0.15	0.18	0.16	0.2	0.25	0.25	0.3	0.36

2.3. Surface wear analysis

Wear rates observed on the tribometer samples were very small, this is important in tribological testing relating to engines to ensure the tribofilms formed from fully-formulated oils are realistic. Optical white light interferometry was used to obtain 3D topography images of the disk sample and ball sample surfaces after tribological tests. The ball sample wear volume was measured with NPFlex 3D Optical Profilometer and obtained data analysed with Vision 64 software from Bruker. To assess the volume loss (V_{wear}) and wear rate (K) after tribological tests wear rate was calculated by Archard expression in Equation (3), where L is the sliding distance and W is the normal load.

$$K = \frac{V_{wear}}{LW}; (3)$$

The typical ball wear topography is shown in Fig. 4a and X-Y profile wear measurements are represented in Fig. 4b.

a) b)

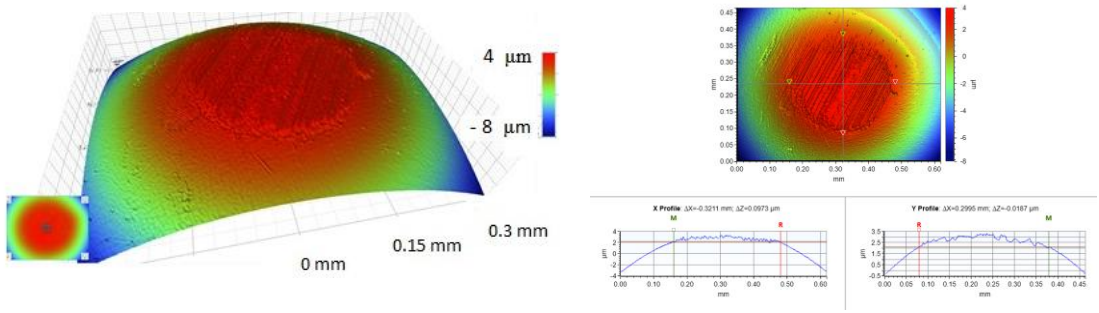

Fig. 4 a) 3D image of the typical wear scar on the ball sample surface, b) X-Y profile wear measurements of the ball sample after ball-on-disk tribological tests.

2.4 Surface chemical characterisation

To remove the residual oil, disk samples after tribometer tests were rinsed with heptane. Residual oil on the sample surface hinders chemical information acquisition, whereas base oil peaks can appear stronger than MoS_2 peaks, in general, making it harder to detect them in a Raman spectrum [11, 12]. Rinsing with a less aggressive solvent allows obtaining sharp tribofilm peaks.

Chemical surface analysis was conducted with Raman Spectroscopy using the inVia Renishaw system. The laser excitation source used was 488 nm wavelength laser with 2400 lines/mm grating. Combined with a 50x Leica optical microscope lens gives 1 µm lateral resolution. Raman laser power was adjusted to avoid damage and thermal energy influence on the tribofilm. Fig. 5. a) shows the optical microscope image from the wear scar scanned. For single-point Raman spectra acquisition, 2 mW laser power was exposed on the sample surface for 1 accumulation and 1 second of exposure time. The Raman spectra of MoS_2 vibration modes at 384 cm^{-1} (E^1_{2g}) and 408 cm^{-1} (A_{1g}) obtained are shown in Fig. 5. b). Tribofilm distribution on the wear scar surface was obtained by Raman mapping. The Raman map is a presentation of the intensity counts of the tribofilm based on the most dominant A_{1g} peak spectral region. The automated platform in the Raman spectrometer allows collection of chemical surface information from the predefined areas on the wear scar. Raman mapping was set to scan a 30 µm x 30 µm area along x and y directions from wear scar centre with a step size of 1 µm, creating 900 acquisition points per single map scan. An example of the mesh grid created over a measuring area of 30 µm x 30 µm is shown in Fig. 5. c). The circular regions at the intersection points shown in Fig. 5. d) are laser source spots from which Raman spectra will be acquired and the distance between two adjacent point is 1 µm that is determined by the step size in x and y directions.

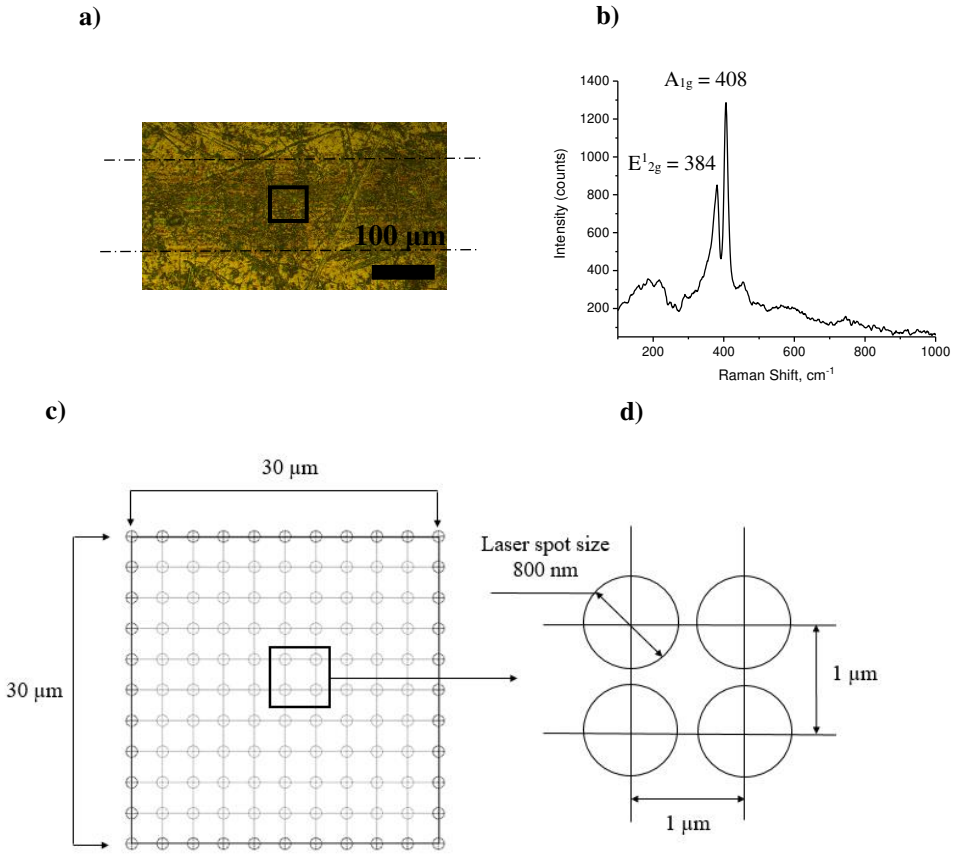

Fig. 5. a) Wear scar on the disk sample after tribometer tests, b) MoS_2 vibrational modes acquired in single-point Raman spectra, c) Schematic diagram showing a mesh created over an area measuring 30 µm x 30 µm, d) Unit dimensions used to create 1 µm x 1 µm of the Raman map.

The laser parameters were kept the same as in single-point analysis modes. Each map was repeated 2 two times, changing the map scan area within the wear scar. Normal laser polarisation was used in this study, because in previous studies [10-12] using different laser polarisations (normal, orthogonal and circular) it was found that there was no influence the acquired E^1_{2g} and A_{1g} peak intensities, rather a slight shift of the A_{1g}/E^1_{2g} peak intensity ratios.

2.5 Raman mapping and intensity histogram development. Laser source influence on the data acquisition

Raman mapping analysis was carried out on a 30 µm x 30 µm area within the wear scar according to the mapping pattern as shown in Fig. 5. Fig. 6 a) shows the Raman map, where each colour pixel in the Raman map represents the A_{1g} intensity counts. The colour of the pixel was determined from a colour scale where low intensity values were blue and high intensity values were red. Each Raman spectrum was assigned to equal width non-overlapping intervals depending on the intensity count and constructed into histogram shown in Fig.6. b) and c). The column size in the histogram shown in Fig. 6. b) presents the peak intensity occurrence frequency (f_n) per single spectrum in a Raman map. To quantify MoS_2 species detected in each Raman map and histogram, area coverage, cumulative intensity, intensity average (mean) and standard deviation parameters were calculated according to the intensity counts acquired during the map scan. The cumulative number was calculated from all intervals and frequencies in Equation (4). The cumulative intensity counts ($\sum$) are all Raman peak intensity cumulated counts detected during the map scan. The frequency per mapping intensity was plotted and correlated depending on the coefficient of friction values, MoDTC concentration, rheology properties of the oil and the lambda ratio conditions**.** Raman intensities below 100 counts were considered as a background signal noise.

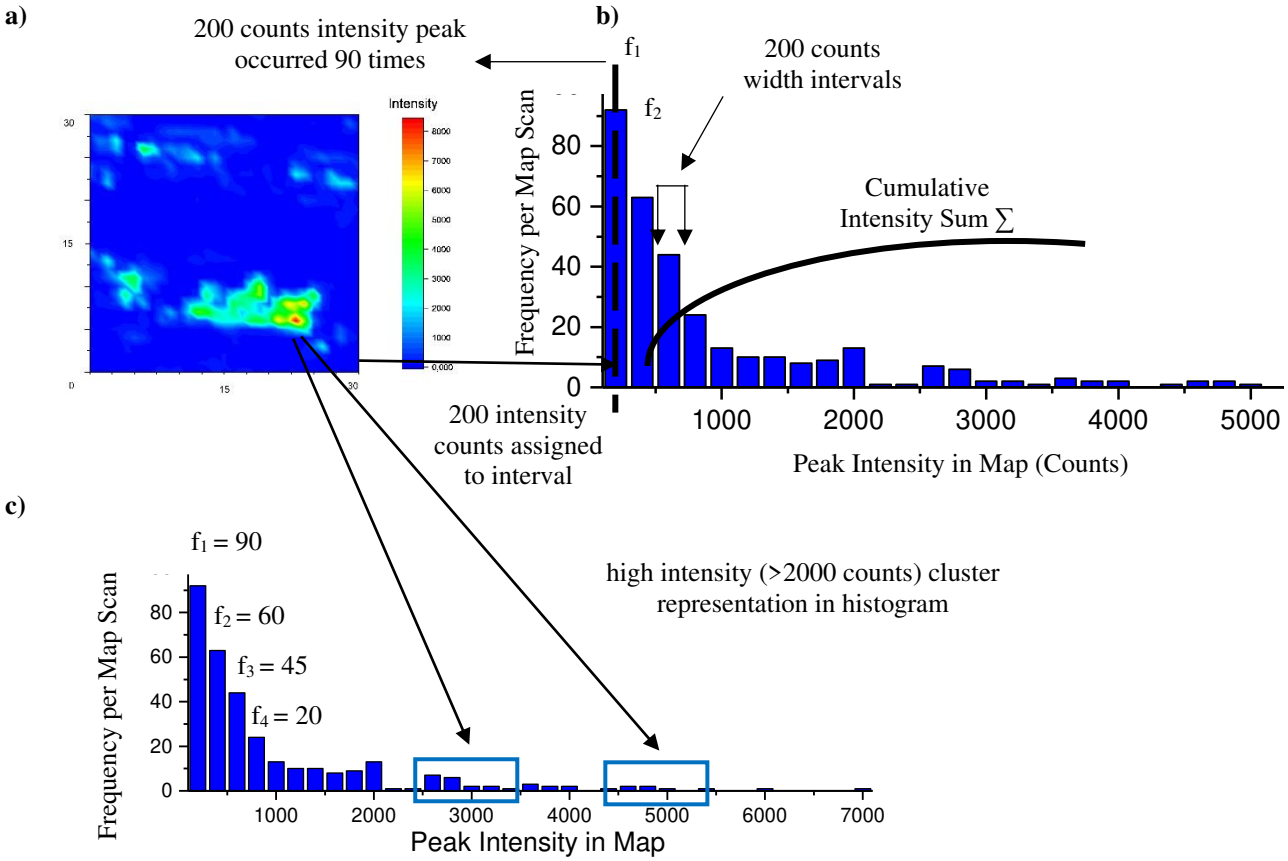

Fig. 6. a) MoS_2 tribofilm Raman map b) Raman map conversion to histogram according to MoS_2 peak intensity counts, c) high intensity tribofilm clusters (>2000 counts) representation with histogram.

$$\sum = 200 \cdot f_1 + 400 \cdot f_2 + 600 \cdot f_3 + \cdots n \cdot f_n \,; (4)$$

Fig. 7 b) and e) show the Raman map developed from different regions (Fig. 7 a) and d)) on the same wear scar surface to assess the homogeneity of the tribofilm. The Raman maps are presented in different colour scales to show the full ranges of the acquired peak intensities. Fig. 7. c) and f) show constructed histograms from Raman maps. One Raman map shows the A_{1g} intensity varies from 100 to 3700 counts in Fig. 7.b) and c) and results in 32.3% area coverage. A second map from a different region is presented in Fig. 7. e) and f) and shows intensity variation from 100 to 8300 counts and 33.5% area coverage. However the total amount of MoS_2 in 3 dimensions can have a substantial variation for a similar 2D surface coverage and, in addition, the mean of the Raman intensity peaks are significantly different. Histograms constructed from Raman maps in Fig. 7. c) and f) reveal a wide intensity distribution in different regions of the wear scar. Due to MoS_2 uneven distribution within the wear scar the fluctuations in cumulative intensity counts can reach 60% while measuring the same sample surface in different locations shown in Table 4. The combination of surface coverage and intensity changes can provide complementary information on the nature of the MoS_2-containing tribofilm. The recorded changes of the acquired data are summarised in Table 4.

For comprehensive analysis all the intensity counts acquired during the Raman map are summarised and compared by the MoS_2 coverage percentage and cumulative histogram intensity number. To visualize the tribofilm distribution across different MoDTC concentrations and Lambda ratios and maintaining the same intensity scale; only the tribofilm clusters between 100-2000 counts are displayed in the maps. The tribofilm clusters that intensity exceed 2000 counts are shown in yellow colour, identifying the highest limit of the intensity scale.

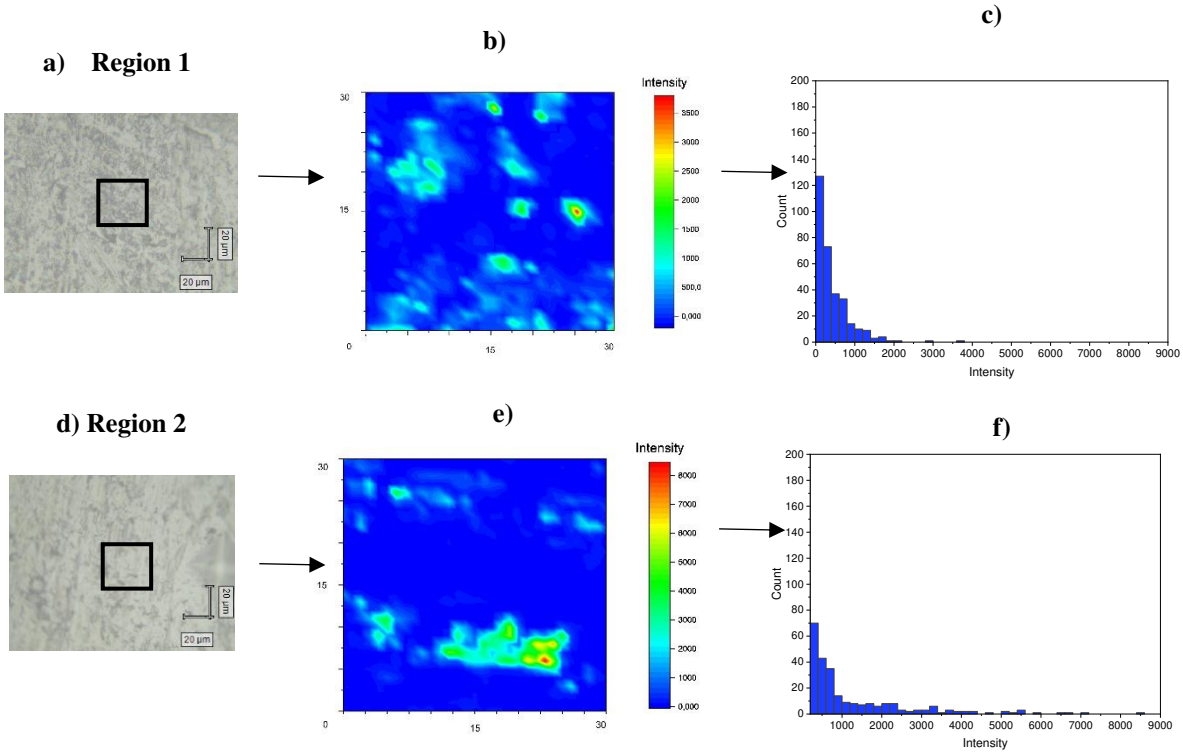

Fig. 7. a), d) Optical images of the wear scar area of the region 1 and 2, b), e) Raman maps of the A_{1g} peak intensity, c), f) Histograms representing peak intensity distribution in the Raman maps.

Table 4. Summary of the Raman mapping measurements acquired from the different regions on the same wear scar surface

	Tribofilm area coverage (%)	A_{1g} peak intensity mean value (counts)	Histogram standard deviation	Histogram Cumulative Intensity (counts)
Region 1	32.3	158	36	199450
Region 2	33.5	313	21	329900

Peak intensities acquired in Raman maps are dependent on the laser source excited energy on the sample surface. To minimise the impact the laser source energy, the laser was calibrated before every measurement session on the standard silicon wafer reference sample. The maximum laser intensity was kept around 37000 to 38000 counts which is equivalent to 8 mW laser source excited energy and equivalent to 2 mW laser energy on the sample surface used for these tests. Before every Raman scan the laser intensity did not drop below 10% of maximum intensity counts value. Table 5 shows the effect that the laser source energy fluctuation would have on MoS_2 tribofilm coverage and intensity. With the laser source energy calibration in Table 5, an 8.9% error in MoS_2 area coverage acquisition and a 3% error in MoS_2 acquired cumulative intensity sum counts were observed. Further Raman mapping analysis is conducted with 30µm x 30µm map dimensions that are deemed to be representative for the tribofilm quantitative analysis.

Table 5. Laser source excited energy fluctuations and its influence on the acquired Raman mapping result

Test time:	Laser source energy (counts)	MoS_2 area coverage (%)	Cumulative intensity sum per map scan (counts)
1 hour	37084	23.6	334800
3 hours	37183	25.9	336700
4 hours	37263	25.2	345200
6 hours	38086	24	343100

3 RESULTS

3.1 MoDTC concentration and nominal lambda ratio influence on friction

A typical characteristic of a friction versus time graph when the MoDTC additive is active shows a drop in friction; this can be after an induction/stabilisation time or can be immediate depending on the type of MoDTC, the concentration and other tribological conditions. Fig. 8 shows the coefficient of friction (COF) dependency on time and MoDTC concentration in the fully-formulated engine oils. When higher MoDTC contents are added to the oil (1% - 0.5%), the stabilisation time is reduced as expected and the time to reach a steady friction value of 0.04 varies from approximately 2 minutes to 10 minutes. When 0.2% of MoDTC is present in the oil the stabilisation time increases up to 15 minutes resulting in a final stabilised friction value of 0.07. The lowest COF value reached is μ=0.04, which has been previously reported in [10, 30] for a typical MoS_2 tribofilm. In Fig. 8 a) and b) it is clear that there is a large difference in behaviour between the oils with no MoDTC additive or a low concentration of 0.2% MoDTC compared to the three higher concentrations which show similar behaviour. The stabilised friction value is the same for the higher concentrations and the only difference is in the time to reach that stabilised value as previously mentioned.

a) HTHS 1.7 (FF oil 1) no VM, λ=0.12 **b) HTHS 1.7 (FF oil1) no VM, λ=0.25**

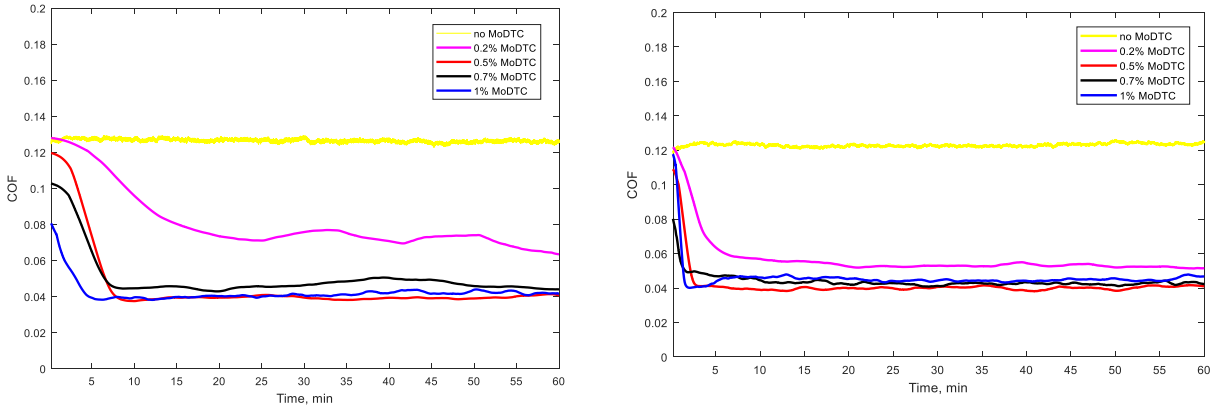

Fig. 8. COF dependency on time and MoDTC concentration a) FF oil 1, η_0 =4.15·10^{-3}(Pa s), HTHS 1.7, no VM added, nominal λ=0.12, b) FF oil 1, η_0 =4.15·10^{-3} (Pa s), HTHS 1.7, no VM added, nominal λ=0.25.

Fig. 9 shows the final coefficient of friction as a function of time and MoDTC content in the fully-formulated engine oil. In 1 hour reference tests in fully-formulated oils without MoDTC, COF values were 0.12-0.13, which changed slightly with increasing speed and a higher lambda ratio. The concentration of MoDTC resulted in significant changes in friction coefficient values. In Fig. 9 it is clear that there is a difference in behaviour between the oils with no MoDTC additive or with MoDTC which is dependent on the viscosity. Without VM (HTHS 1.7) it is clear that for the two highest concentrations of MODTC (0.7% and 1%) the final friction coefficients are comparable and are independent of the Lambda ratio. At the higher viscosity (HTHS

2.1) the concentrations of 0.5%, 0.7% and 1% all show low and comparable friction, independent of Lambda ratio. For HTHS 3 the situation is slightly different. At the lowest Lambda ratio the friction steadily decreases as the concentration of MoDTC increases while at the higher Lambda ratios the two highest concentrations of 0.7% and 1% show similar behaviour.

a) HTHS 1.7 (FF oil 1) no VM

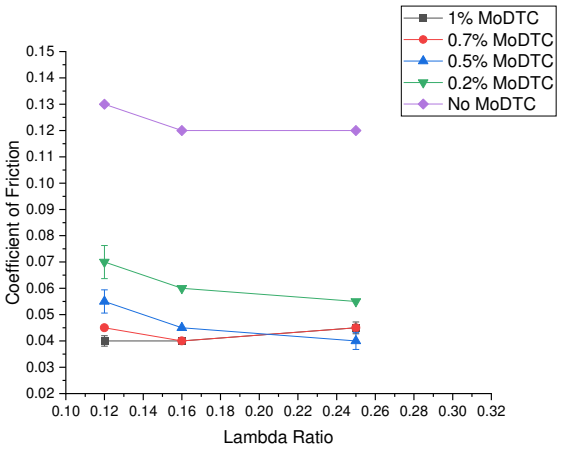

b) HTHS 2.1 (FF oil 2) with VM

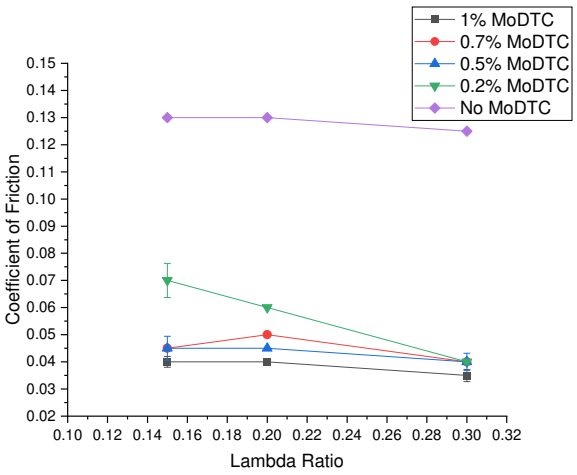

c) HTHS 3 (FF oil 3) with VM

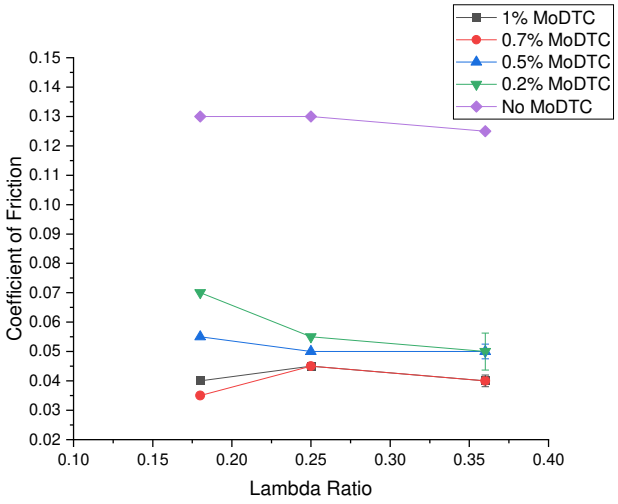

Fig. 9. COF dependency on nominal λ ratio and MoDTC concentration in fully-formulated engine oils. a) FF oil 1, η_0 =4.15·10^{-3} (Pa s), HTHS 1.7, no VM added, b) FF oil 2, η_0=5.76·10^{-3} (Pa s), HTHS 2.1, with VM, c) FF oil 3, η_o=9.12·10^{-3} (Pa s), HTHS 3, with VM.

Friction trends are therefore shown to be dependent on the MoDTC concentration, the lambda ratio and also the addition of VM. This is likely to be at least in part due to the differences in the tribofilm formation. The next sections examine the tribofilm formation with the primary function being to understand exactly what influence the quantity and the distribution of MoS_2 has on the friction behavior.

3.2 Wear analysis

Wear generated on the disk and ball samples was small, even with the Hertzian contact pressure of 0.72 GPa and the low viscosity oils. It shows the excellent functionality of the anti-wear additives in the fully-formulated oils. The wear scar diameter on the ball samples and wear track profiles on disks were compared between different MoDTC concentration tests and the lambda ratio. On average at least three measures were made for each wear scar area.

Wear scars on the disk and ball samples were formed as shown in Fig. 10. a. and Fig. 10. b. White light interferometry measurements were conducted on the disk samples wear tracks, which were micro indented before analysis for measurement area tracking purposes. Fig. 10. c. shows white light interferometry measures of the wear track profiles at nominal λ= 0.15 at 40 rpm speed. On average, wear track width is 100 µm across all fully-formulated oil viscosities and additive concentrations. Wear track profile measures do not show a change in the surface roughness inside and outside wear scar. Measures on the disk samples did not reveal a correlation in the wear when low oil viscosity changes from $\eta_0 = 4.15 \cdot 10^{-3}$ (Pa s) (FF oil 1) to $\eta_0 = 9.12 \cdot 10^{-3}$ (Pa s) (FF oil 3).

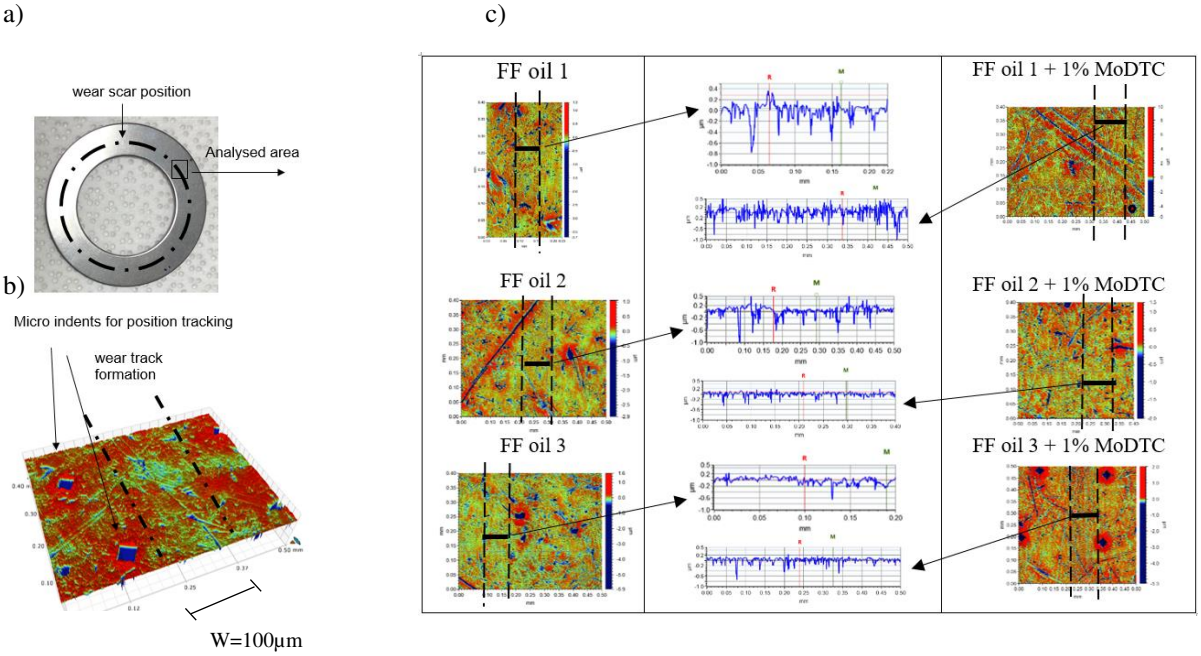

Fig. 10 a) wear scar formation after tribometer tests on disk sample, b) wear track surface and micro indentation (FF oil 1 0.2% MoDTC λ=0.15), c) wear track profile comparison between tests with FF oils and FF oils+ 1% MoDTC.

Fig. 11 shows the wear rate measured from the ball samples after 1 hour tests. The highest wear observed was in the tests with low viscosity FF oil 1. Tests with lowest viscosity oil experience oil film thinning that exposes the rubbing surfaces to more severe asperity contact which leads to a higher wear. Wear reduction is observed when polymeric viscosity modifier is added to FF oil 2 and FF oil 3 that increased oil viscosity and reduced contact at the asperities.

In general wear rate is reduced by increasing the speed and moving to the higher lambda ratio regions that has less asperities contact that is in good agreement with wear reduction observations previously reported in [31].

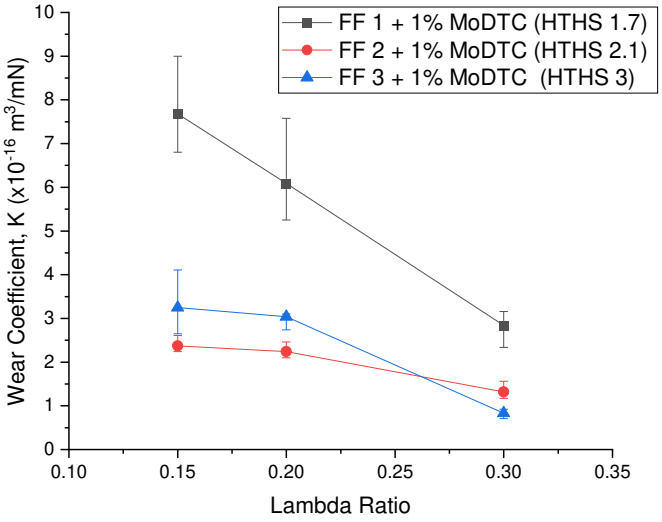

Fig. 11 Wear rate dependency on fully-formulated oil chemistry and nominal λ ratio conditions. Similar trends were observed in the oils with lower MoDTC concentrations.

In this study, the focus is on MoS_2 tribofilm formation and its influence on the friction behaviour and quantitative chemical surface characterization. Important conclusion of the wear analysis is wear experienced after 1 hour long tests in fully-formulated oils is very small and MoDTC content in the oil does not influence the wear changes greatly, which is in a good agreement with previously conducted studies [21, 22, 31, 32].

3.3 MoS_2 tribofilm characterisation

Mapping measurements were made on all samples at the end of the one-hour tests. In this paper, to illustrate how the tribofilm characteristics change and how we will evaluate this, the most extreme cases were chosen: tests with the highest and lowest MoDTC contents and sliding speeds resulting in stabilised friction values of 0.07 at low concentration and low speed and 0.04 at high concentration and high speed. Figs 12 - 14 show the MoS_2 tribofilm distribution on disk sample wear scars tested using FF oil 1, FF oil 2 and FF oil 3 respectively. Fig.12. a) shows that the smallest area coverage, occurred in low speed and low MoDTC concentration test conditions. When the speed was increased, tribofilm area coverage increased to 36% (Fig. 12. b).), resulting in reduced friction value. Highest MoS_2 tribofilm coverage was obtained during tests with 1% MoDTC concentration in the oil in the Fig. 12. c). and Fig. 12. d), reducing further the final friction value to μ=0.04.

With the MoS_2 tribofilm coverage increasing from 18% to 36%, the influence of sliding speed on MoS_2 tribofilm formation was seen to be greater when the low MoDTC concentration oil was tested. This observation is noticed in the Raman map histograms as well. Fig. 12. e). and Fig. 12. f). show the histograms of MoS_2 peak intensities obtained from the maps shown in Fig. 12. a) to d). The tests that provided lowest COF values, higher MoDTC concentration, show a wider range of MoS_2 peak intensity counts (>2000), although their frequency is not high. The highest cumulative counts are acquired on the samples formed in 1% MoDTC concentration, which provided the highest friction reduction.

λ Ratio Influence (range 0.12-0.25)

a) Area coverage 18%, μ=0.07, Cumulative Intensity Sum 77400 counts

b) Area coverage 36%, μ= 0.055, Cumulative Intensity Sum 319400 counts

0.2% MoDTC

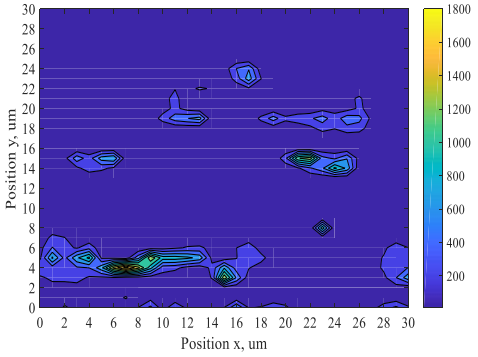

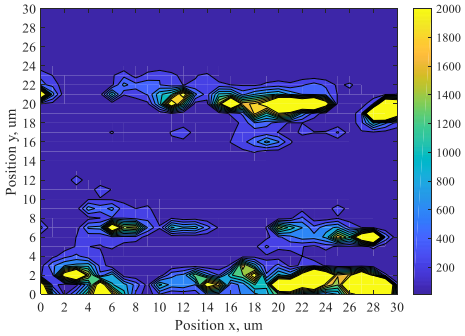

c) Area coverage 41%, μ=0.04, Cumulative Intensity Sum 374000 counts

d) Area coverage 47%, μ=0.04, Cumulative Intensity Sum 525600 counts

1% MoDTC

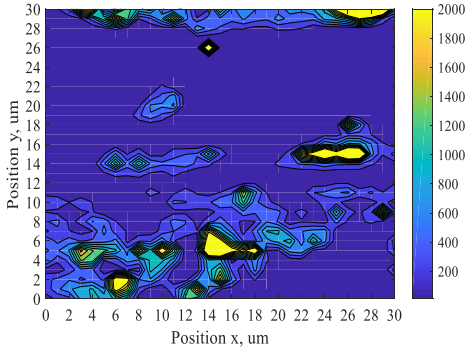

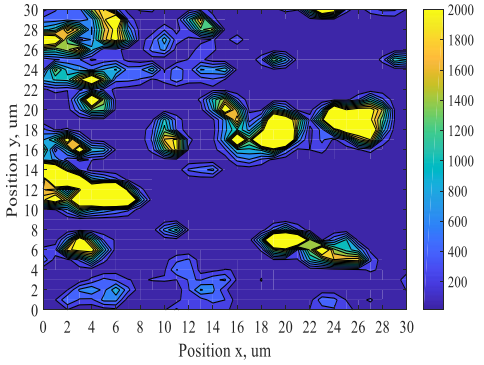

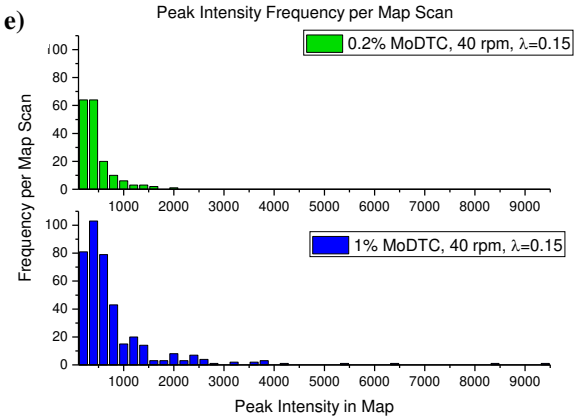

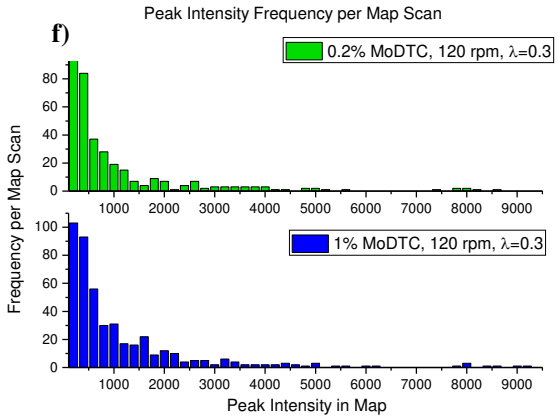

Fig. 12 Raman maps conducted on the disk wear scar from tests in FF oil 1, η_0 =4.15·10^{-3} (Pa s), HTHS 1.7, no VM added a) λ ratio=0.12, 0.2 % MoDTC, b) λ ratio=0.25, 0.2 % MoDTC, c) λ ratio=0.12, 1% MoDTC d) λ ratio=0.25, 1% MoDTC, e)-f) Histograms presenting maps a)-d) respectively.

When a viscosity modifier is added in the oil FF 2, the dynamic viscosity increased to $\eta_0=5.76\cdot10^3$ (Pa s). Fig. 13 a) and b) show similar area coverage trends to the ones observed in FF oil 1 in 0.2% MoDTC concentration (in Fig. 12. a) and b)). The smallest area coverage of 15% is noticed in Fig.13. a., in a low speed and a low MoDTC concentration test conditions. Increasing the testing speed resulted in higher MoS_2 coverage of 34% (Fig. 13. b) and final friction value reduction from μ=0.07 to μ=0.04 respectively. Histograms in Fig. 13. e). and Fig. 13. f). reveal that increase in the lambda ratio and MoDTC concentration leads to the reduction of high intensity MoS_2 peaks. Interestingly the cumulative counts and area coverage observed appear to drop, although the observed tribofilm amount is sufficient enough to support μ= 0.04 final friction value. The observed link between low friction value and MoS_2 coverage and cumulative intensity reduction is explained in the discussion section.

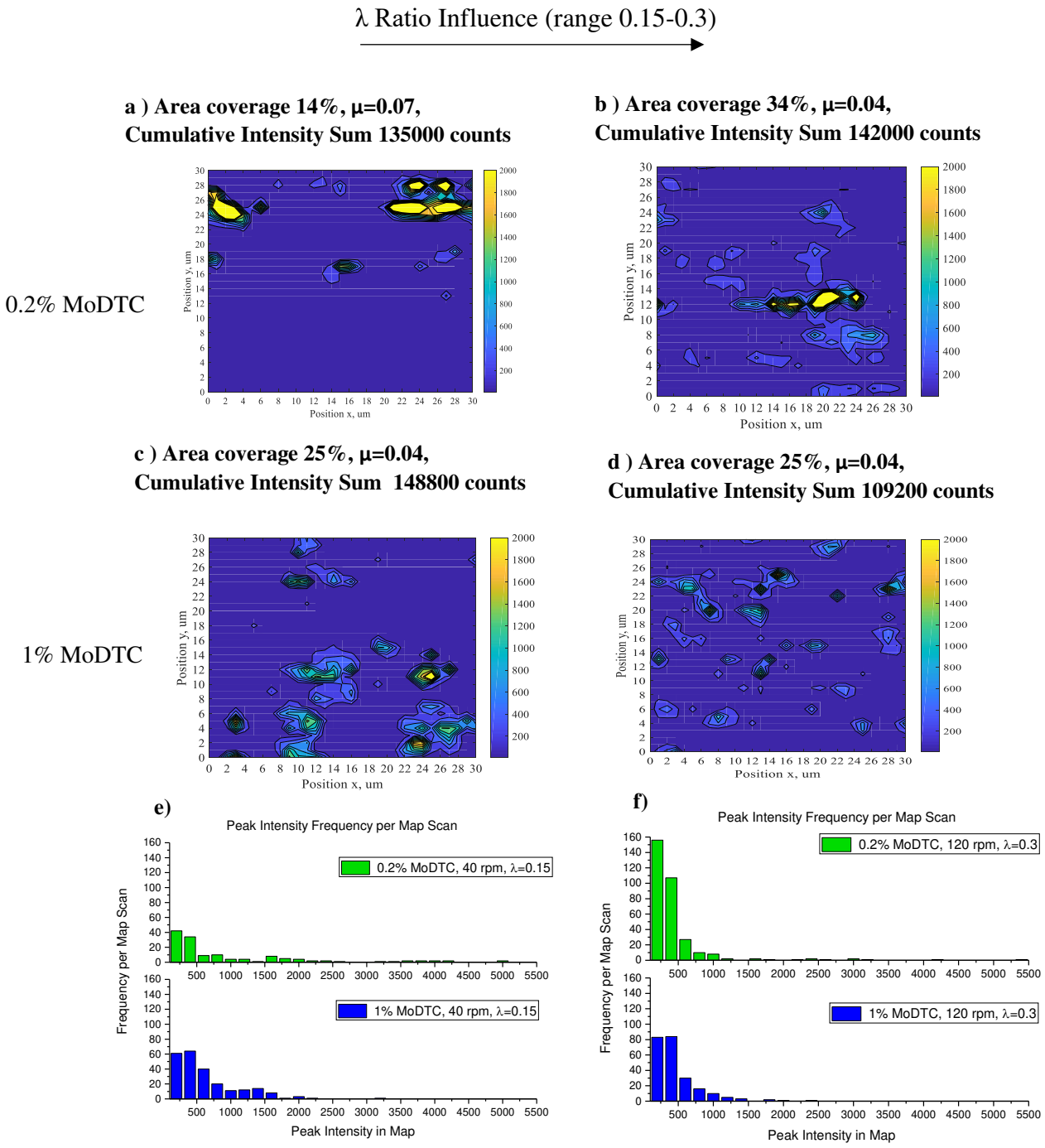

Fig. 13 Raman maps conducted on the wear scar from tests in FF oil 2, $\eta_0=5.76\cdot10^{-3}$ (Pa s), HTHS 2.1, with VM added a) λ ratio=0.15, 0.2 % MoDTC, b) λ ratio=0.3, 0.2 % MoDTC, c) λ ratio=0.15, 1%

MoDTC d) λ ratio=0.3, 1% MoDTC, e)-f) Histograms presenting maps a)-d) respectively.

Fig. 14. shows the tribofilm formation and distribution from the tests with FF oil 3 which has the highest dynamic (η_0=9.12·10^{-3} (Pa s)) and HTHS viscosity (3 cP) from all the tested oils. In general, the MoS_2 tribofilm is built more uniformly, considering that the area coverage between all tests is measured to be within 23% - 34% range, in comparison to FF oil 1 area coverage 18% - 47% and FF oil 2 - 15% - 35%. Although the tribofilm coverage and cumulative intensity numbers do not vary greatly, there is a difference in friction behaviour.

The highest area coverage is obtained at tests in higher MoDTC concentration shown in Fig 14 c) and d) resulting in μ=0.04 final friction value. Speed increase in the tribocontact shown in Fig. 14 b) and d) reveals the tribofilm area coverage reduction in both MoDTC concentrations, which is a reverse trend on what has been observed in tests with lower viscosity FF oil 1 and FF oil 2. Histograms in Fig 14 e) and f) show the same trend as Raman maps, the highest intensities (>2000 counts) are obtained in low speed and high MoDTC concentration conditions resulting in 311600 cumulative intensity counts and μ=0.04 final friction value. The increase in the lambda ratio resulted in a significant reduction in cumulative intensity counts from 96400 to 159200 counts, while providing reduced friction of μ=0.05 and μ=0.04 respectively. The potential mechanisms for this performance will be discussed in the next section.

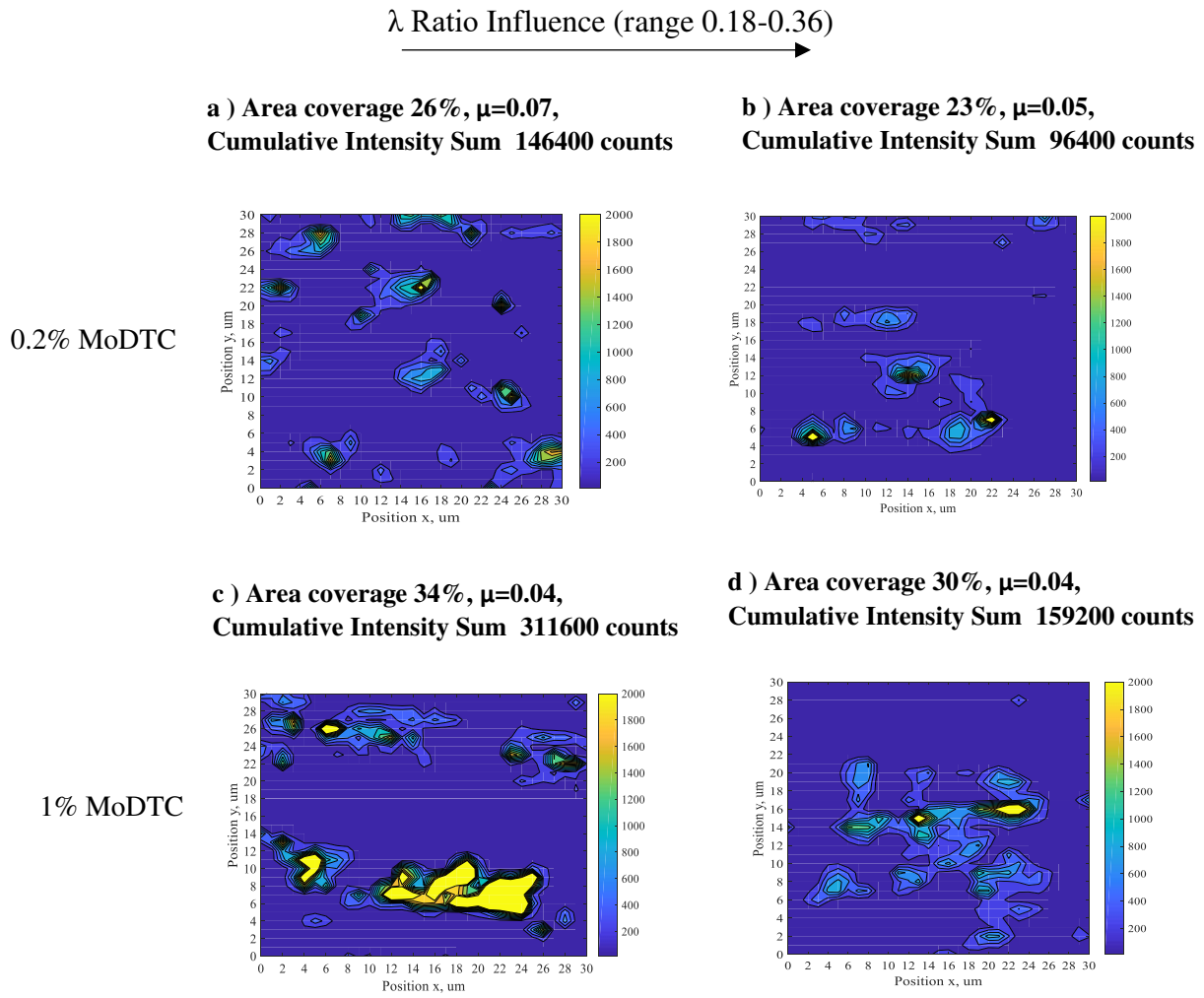

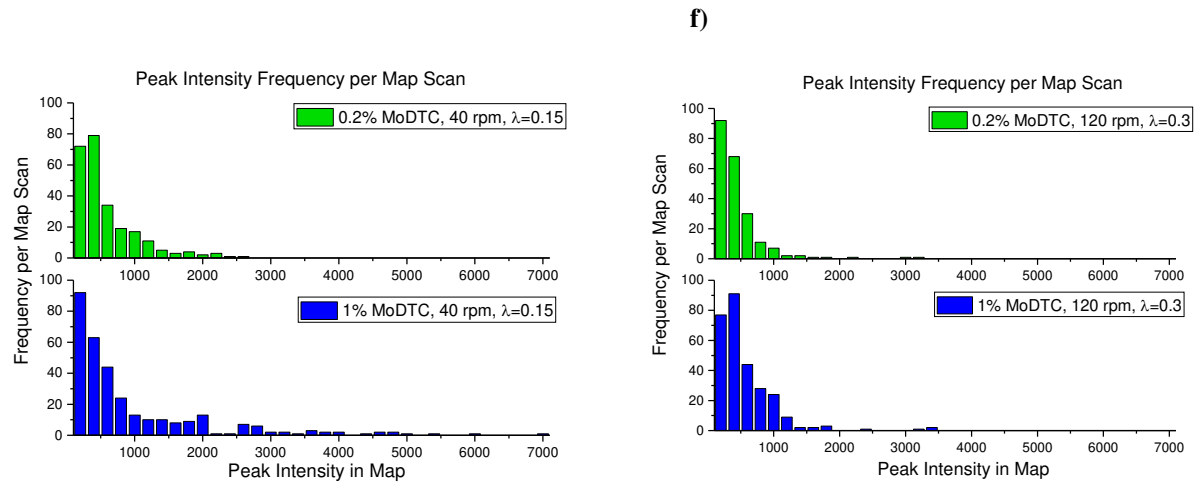

Fig. 14 Raman maps conducted on the wear scar on the sample surface from tests in FF oil 3, $\eta_0=9.12\cdot10^{-3}$ (Pa s), HTHS 3, with VM added a) λ ratio=0.18, 0.2 % MoDTC, b) λ ratio=0.36, 0.2 % MoDTC, c) λ ratio=0.18, 1% MoDTC d) λ ratio=0.36, 1% MoDTC, e)-f) Histograms presenting maps a)-d) respectively.

The Raman maps confirm that viscosity modifier presence in the fully-formulated oil has a significant role in determining the nature of the MoS2 tribofilm. This information complements the previously-presented friction and wear data that show that the concentration of MoDTC, the tribological conditions also play a role. The observed link between low final friction value, MoS_2 coverage and cumulative intensity is explained in the discussion section. The following discussion presents MoDTC friction behaviour and resulting MoS_2 tribofilm spatial distribution trends in fully-formulated low viscosity oils.

4 DISCUSSION

4.1 The effect of oil viscosity and polymeric viscosity modifier on friction in boundary lubrication

Studies on viscosity modifier influence on oil viscosity and friction behaviour are mostly conducted in EHL regime conditions [36-39]. In EHL conditions, a continous lubricant film will separate the surfaces and due to lack of asperity contact, the MoDTC is not decomposed to form MoS_2. It has been shown by other researchers that when viscosity modifier was added into the oil and the speed in the tribological contact was reduced, the MoDTC effect on friction reduction was noticed [40, 41].

In this work when MoDTC additive is introduced to fully-formulated oils, as expected, the COF was reduced to lower values. Tests with a higher MoDTC concentration (0.5% - 1% with VM and 0.7%-1% without VM) reduced the COF to 0.04-0.05 which is typical for a MoS_2 tribofilm [10, 30]. Fig. 8 and Fig. 9 show that the effect of MoDTC concentration on friction performance also depends on the sliding speed. Sliding speed is one of the parameters which defines the fluid film thickness and as a consequence the extent of asperity contact. Considering that the formation of MoS_2 sheets is accelerated by the contact at surface asperities [10], the thinner fluid film will result in a higher rate of MoS_2 tribofilm formation but also in a higher tribofilm removal rate. When testing speed increases from 40 rpm to 120 rpm, the lambda ratio shifts from a severe boundary regime at 0.12 to 0.25, resulting in a slightly thicker fluid film. Maps of the MoS_2 tribofilm formed, shown in Fig. 12. a) and b), indicate that higher sliding speed promotes MoS_2 tribofilm formation on the wear scar even from the oil with low MoDTC concentration, explaining the further reduction of friction to 0.055.

High molecular weight polymeric VM molecules expand with temperature [24, 25, 35] and as a result will alter the viscosity at the asperity contact, an effect which will not be captured by the nominal lambda ratio. Fig. 9. b) and c) show that the presence of VM in FF oil 2 and FF oil 3 gives low friction even with 0.5% of MoDTC at low nominal lambda ratio, while at higher speeds, low friction is achieved with 0.2% of MoDTC too.

4.2 MoS_2 formation, spatial distribution (coverage) and total intensity in different viscosity fully formulated oils

Raman spectroscopy has been established as an effective technique to characterize tribofilms formed from Mo-containing oils. In some published papers [10, 44], a very neat correlation between the MoS_2 coverage (2D), intermediate amorphous Mo species and friction were observed. In this paper a number of variables including the MoDTC concentration, the presence/absence of VM and the tribological parameters have been probed and their effects on the MoS_2 tribofilm assessed. What arises from this is that the situation is complex and that there is not a universal relationship between friction and either coverage, Raman peak intensity or cumulative intensity. This is best illustrated in Fig. 15 a) and b) where the COF is plotted against the coverage and the cumulative intensity. From Figure 15 a) and b) some important contributions to the understanding of MoS_2-containing tribofilms become clear:

1. MoS_2 tribofilm coverage and cumulative intensity counts suggest that oil viscosity has a significant influence on the tribochemistry in the contact. In the lower viscosity oil, the tribofilm coverage (Fig 15 a)) and cumulative intensity (Fig 15 b)) both show a clear linear relationship with the achieved friction value - this trend is weakened in higher viscosity oils. Interestingly in higher viscosity oils whether the friction is high (μ=0.07) or low (μ=0.04) does not seem to be represented by a correlation with coverage or cumulative intensity.

2. At higher viscosity it would appear that other factors are important in determining the value of friction coefficient and it is postulated that the observed reduction of MoS_2 on the wear scar can be effected by many factors such as tribofilm formation from other additives in the oil, tribofilm structure changes, and in general asperity contact reduction in higher viscosity oils. The MoDTC additive is known to decompose upon high shearing on the steel/steel surface asperities. The AFM study conducted in [42] observed that there is a strong relationship between asperity contact and friction behaviour in the boundary regime. AFM observations showed that MoS_2 sheets form on the load carrying surface asperities in the contact. The study suggested that as long as the key asperities are covered with MoS_2 sheets the friction reduction can be controlled in the boundary regime. Complementary studies have shown that when a layered MoS_2 tribofilm is formed, as evidenced by FIB and TEM images in [13], and more recently in [43], friction reduction can occur. It would appear in this current study that although MoS_2 tribofilm coverage and intensity for thicker oils is lower, the friction reduction is achieved by the formation of MoS_2 tribofilm layers on the wear scar.

3. Another important aspect to consider is the synergetic and antagonistic effects of other additives in the fully formulated oil. Guegan et al. [39] reported that VM in high temperature conditions in the base oil is more effective than in fully-formulated oils, suggesting that VM can have synergetic and antagonistic effects with friction modifiers and other additives in the oil.

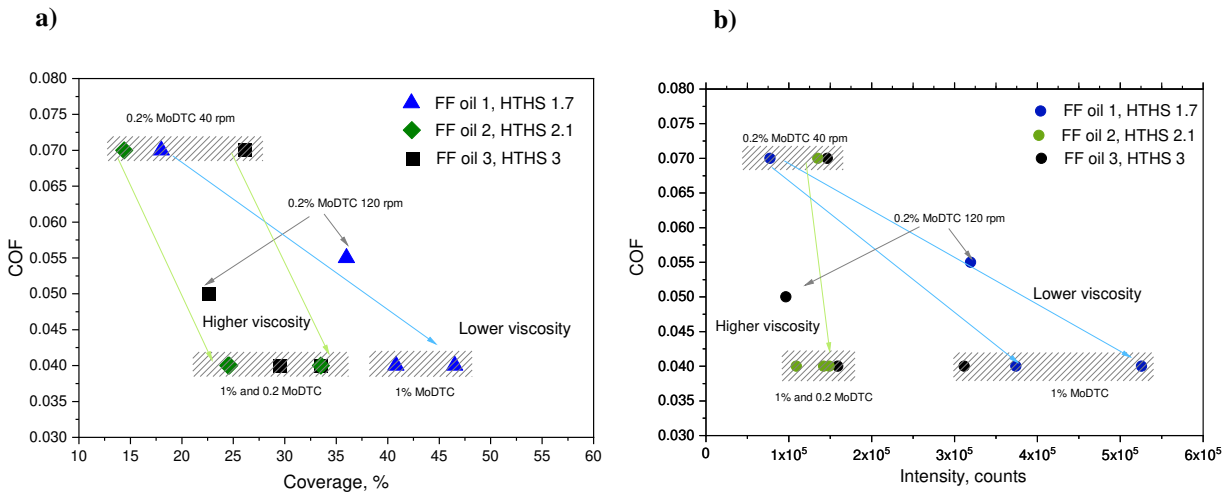

Fig. 15 Fully-formulated oil viscosity influence on MoS_2 tribofilm distribution. a) COF as a function of the area coverage, b) COF as a function of the cumulative intensity counts.

5 CONCLUSIONS

In this study, fully formulated oils containing different concentrations of MoDTC were tested with and without VM additives. Using Raman spectroscopy the 2D coverage of MoS_2 and the cumulative intensity (related to the 3D amount in the analysed volume) were assessed in relation to the friction of the tribocontact. The main conclusions are:

1. At higher MoDTC concentrations (0.5% - 1% with VM and 0.7%-1% without VM) COF values were independent of the Lambda ratio and the low values of 0.04 were achieved.
2. The sliding distance prior to stable friction, the stabilisation period, is seen to be dependent on the concentration of the MoDTC.
3. All low viscosity fully formulated oil combinations tested in this study gave very small wear, and the MoDTC concentration in the oil did not affect the wear performance.
4. There is not a universal correlation between MoS_2 surface coverage and friction nor between cumulative MoS_2 intensity and friction. In low viscosity oils there is a general trend that higher coverage and cumulative intensity correlate to lower friction. This is not seen for higher viscosity oils.
5. For higher viscosity oils it is postulated that the differences in friction seen for common Raman intensity/coverage values arise because of the ordering of the layered structure of the MoS_2 tribofilm.

REFERENCES

[1] European Environment Agency (EEA) report (2018), Greenhouse gas emissions from transport in Europe. Retrieved from https://www.eea.europa.eu/data-and-maps/indicators/transport-emissions-of-greenhouse-gases/transport-emissions-of-greenhouse-gases-11. (05/09/2019)

[2] U.S. Environmental Protection Agency (EPA) report (2017), Sources of Greenhouse Gas Emissions. Retrieved from https://www.epa.gov/ghgemissions/sources-greenhouse-gas-emissions. (05/09/2019).

[3] Qu J, Luo H, Chi M, Ma C, Blau PJ, Dai S, et al. Comparison of an oil-miscible ionic liquid and ZDDP as a lubricant anti-wear additive. Tribol Int 2014; 71:88–97.

[4] Heywood, J., Internal Combustion Engine Fundamentals. McGraw-Hill Education, 1988.

[5] Holmberg, K., Andersson, P., Nylund, N. O., Mäkelä, K. and Erdemir, A. "Global energy consumption due to friction in trucks and buses," Tribology International, vol. 78, pp. 94–114, 2014.

[6] Hamid, Y., Usman, A., Kamran, A. Cheol Woo Park, Numeric based low viscosity adiabatic thermos tribological performance analysis of piston-skirt liner system lubrication at high engine speed, Tribology International, Volume 126, 2018, Pages 166-176.

[7] Rudnick, L. Lubricant additives: chemistry and applications. CRC Press, 2010.

[8] Robinson, J., Zhou, Y., Bhattacharya, P., Erck, R., Qu, J., Bays, T. and Cosimbescu, L. "Probing the molecular design of hyper-branched aryl polyesters towards lubricant applications," Scientific Reports,vol. 6, no. November 2015, pp. 1–10, 2016.

[9] Hsu, S. M. "Molecular basis of lubrication," Tribology International, vol. 37, no. 7, pp. 553 – 559, 2004.

[10] Xu D., Wang C., Espejo C., Wang J., Neville A. and Morina A., "Understanding the friction reduction mechanism based on the molybdenum disulfide tribofilm formation and removal," Langmuir, vol. 34, 10 2018.

[11] Khaemba, D. N.; Neville, A.; Morina, A. New insights on the decomposition mechanism of Molybdenum DialkyldiThioCarbamate (MoDTC): a Raman spectroscopic study. RSC Adv. 2016, 6 (45), 38637−38646.

[12] Khaemba, D., Neville, A. and Morina, A., A methodology for Raman characterisation of MoDTC tribofilms and its application in investigating the influence of surface chemistry on friction performance of MoDTC lubricants, Tribol. Lett., 2015, 59(3), 1–17.

[13] Rai Y, Neville A, Morina A. Transient processes of MoS_2 tribofilm formation under boundary lubrication. Lubric Sci 2016;29:449–71.

[14] Balarini, R., Diniz, G.A.S., Profito, F.J., Souza, R.M. Comparison of unidirectional and reciprocating tribometers in tests with MoDTC-containing oils under boundary lubrication, Tribology International, 2019.

[15] Kosarieh, S., Morina, A., Lainé, E., Flemming, J., Neville, A. Tribological performance and tribochemical processes in a DLC/steel system when lubricated in a fully formulated oil and base oil, Surface and Coatings Technology, Volume 217, 2013,Pages 1-12.

[16] Khaemba, D., Frederic, J., Thiebaut, B., Neville, A., Morina, A. (2017). The role of surface roughness and slide-roll ratio in the decomposition of MoDTC in tribological contacts. Journal of Physics D: Applied Physics.
[17] Khaemba, D., Azam, A., See, T., Neville, A., Salehi, F. Understanding the role of surface textures in improving the performance of boundary additives, part I: Experimental,Tribology International, Volume 146, 2020.
[18] Azam, A., Dorgham, A., Khaemba, D., Salehi, F., See, T., Neville, A. Understanding the role of surface textures in improving the performance of boundary additives, part II: Numerical simulations, Tribology International, 2020.
[19] Okubo, H., Sasaki, S., In situ Raman observation of structural transformation of diamond-like carbon films lubricated with MoDTC solution: Mechanism of wear acceleration of DLC films lubricated with MoDTC solution, Tribology International, Volume 113, 2017, p. 399-410.
[20] Okubo, H., Tadokoro, C., Sumi, T., Tanaka, N., Sasaki, S. Wear acceleration mechanism of diamond-like carbon (DLC) films lubricated with MoDTC solution: Roles of tribofilm formation and structural transformation in wear acceleration of DLC films lubricated with MoDTC solution, Tribology International, Volume 133, 2019, p. 271-287.
[21] Masuko, M.,Ono, T., Aoki, S.,Suzuki, A., Ito, H. Friction and wear characteristics of DLC coatings with different hydrogen content lubricated with several Mo-containing compounds and their related compounds, Tribology International, Volume 82, Part B, 2015, p. 350-357.
[22] Muraki, M., Yanagi, Y., and Sakaguchi, K. "Synergistic effect on frictional characteristics under rolling-sliding conditions due to a combination of molybdenum dialkyldithiocar-bamate and zinc dialkyldithiophosphate," Tribology International, vol. 30, no. 1, pp. 69– 75, 1997.
[23] Konicek, A. R., Jacobs, P. W., Webster, M. N. and Schilowitz, A. M., "Role of tribofilms in wear protection," Tribology International, vol. 94, pp. 14 – 19, 2016.
[24] Mary, C., Philippon, D., Devaux, N., Fillot, N., Laurent, D., Bair, S., Vergne, P. "Bridging high pressure rheology and film-forming capacity of polymer-base oil solutions in EHL", Tribology International, Volume 93, Part B, 2016, pp. 502-510.
[25] Mary, C., Philippon, D., Lafarge, L., Laurent, D., Rondelez, F., Vergne, P. *et al.* New insight into the relationship between molecular effects and the rheological behavior of polymer-thickened lubricants under high pressure, Tribol Lett, 52 (2013), pp. 357-369.
[26] Chen, Q.; Cao, X.; Xu, Y.; An, Z. Emerging Synthetic Strategies for Core Cross Linked Star (CCS) Polymers and Applications as Interfacial Stabilizers: Bridging Linear Polymers and Nanoparticles. Macromol. Rapid Commun. 2013, 34, 1507-1517.
[27] Dowson, D. and Higginson, G. R. A numerical solution to the elastohydrodynamic problem. J. Mech. Eng. Sci.,1959, 1,6.
[28] Dowson, D., Higginson, G. R.,and Whitaker, A. V. Elasto-hydrodynamical lubrication: a survey of isothermal solutions. J. Mech. Eng. Sci., 1961, 4, 121–126.
[29] Dowson, D. and Higginson, G.R. Elastohydrodynamic lubrication, the fundamentals of roller and gear lubri-cation, 1966 (Pergamon Press, Oxford, Great Britain).
[30] de Barros' Bouchet, M. I.; Martin, J. M.; Le-Mogne, T.; Vacher, B. Boundary lubrication mechanisms of carbon coatings by MoDTC and ZDDP additives. Tribol. Int. 2005, 38 (3), 257−264.
[31] Morina, A Neville, JH Green, M Priest, Assessing friction, wear and film formation characteristics in formulated lubricants in severe to moderate boundary lubrication conditions, Editor(s): D. Dowson, M. Priest, G. Dalmaz, A.A Lubrecht, Tribology Series, Elsevier, Volume 41, 2003,Pages 23-33.
[32] Espejo, C, Thiebaut, B, Jarnias, F et al. (2019) MoDTC Tribochemistry in Steel/Steel and Steel/Diamond-Like-Carbon Systems Lubricated With Model Lubricants and Fully-formulated Engine Oils. Journal of Tribology, 141 (1).
[33] McDevitt N T, Zabinski J S, Donley M S and Bultman J E 1994 Disorder-induced low-frequency Raman band observed in deposited MoS2 films Appl. Spectrosc. 48 733–6.
[34] McDevitt N T, Bultman J E and Zabinski J S 1998 Study of amorphous MoS_2 films grown by pulsed laser deposition Appl. Spectrosc. 52 1160–4.
[35] Glass, J. E., Schulz, D. N. and Zukoski, C. F.. Polymers as Rheology Modifiers. ACS, Washington DC, 1991
[36] Margareth Judith Souza de Carvalho, Peter Rudolf Seidl, Carlos Rodrigues Pereira Belchior, José Ricardo Sodré, Lubricant viscosity and viscosity improver additive effects on diesel fuel economy, Tribology International, Volume 43, Issue 12, 2010, p. 2298-2302.
[37] Devlin MT, Wy L, Mcdonnell TF. Critical oil properties that control fuel economy in general motors vehicles. SAE Technical Paper SAE 1998; 982503.
[38] Coy, R.C. Practical applications of lubrication models in engines. Paper presented at the World Tribology Congress, London, September 1997.1, Tribology International, Volume 31, Issue 10, 1998, p. 563-571.

[39] Guegan, J., Southby, M. & Spikes, H. Friction Modifier Additives, Synergies and Antagonisms. Tribol Lett 67, 83 (2019).
[40] Smeeth, M., Gunsel, S. and Spikes, H.A. (1996), "Boundary Film Formation by Viscosity Index Improvers." Trib. Trans. 39,pp. 726-734.
[41] Fan, J., Müller, M., Stöhr, T. et al. Reduction of Friction by Functionalised Viscosity Index Improvers. Tribol Lett 28, 287–298 (2007).
[42] Miklozic, K., Graham, J. & Spikes, H. Chemical and Physical Analysis of Reaction Films Formed by Molybdenum Dialkyl-Dithiocarbamate Friction Modifier Additive Using Raman and Atomic Force Microscopy. Tribology Letters 11, 71–81 (2001).
[43] De Barros Bouchet, M.I., Martin, J.M., Oumahi, C., Gorbatchev, O., Afanasiev, P., Geantet, C., Iovine, R., Thiebaut, B., Heau. C.. Booster effect of fatty amine on friction reduction performance of Mo-based additives, Tribology International, Volume 119, 2018, Pages 600-607.
[44] Oumahi, C., De Barros-Bouchet, M. I., Le Mogne, T., Charrin, C., Loridant, S., Geantet, G., Afanasiev, P., Thiebaut, B. MoS_2 formation induced by amorphous MoS_3 species under lubricated friction, RSC Adv., 2018, 8, 25867.